Cancer Biology

FAK loss reduces BRAF^{V600E}-induced ERK phosphorylation to promote intestinal stemness and cecal tumor formation

Chenxi Gao, Huaibin Ge, Shih-Fan Kuan, Chunhui Cai, Xinghua Lu, Farzad Esni, Robert E. Schoen, Jing H. Wang, Edward Chu, Jing Hu

Division of Gastroenterology, Hepatology and Nutrition, Department of Medicine, University of Pittsburgh School of Medicine, Pittsburgh, PA 15213 • UPMC Hillman Cancer Center, Division of Hematology and Oncology, Department of Medicine, University of Pittsburgh, Pittsburgh, PA, 15213, USA • Department of Pathology, University of Pittsburgh School of Medicine, Pittsburgh, PA 15213 • Department of Biomedical Informatics, University of Pittsburgh, Pittsburgh, PA 15206 • Department of Surgery, University of Pittsburgh School of Medicine, Pittsburgh, PA 15213 • Current address: Albert Einstein Cancer Center, Albert Einstein College of Medicine, Bronx, NY 10461

Reviewed Preprint

Published from the original preprint after peer review and assessment by eLife.

About eLife's process

Reviewed preprint version 1
April 3, 2024 (this version)

Sent for peer review
January 5, 2024

Posted to preprint server
February 1, 2023

https://en.wikipedia.org/wiki/Open_access
Copyright information

Abstract

BRAF^{V600E} mutation is a driver mutation in the serrated pathway to colorectal cancers. BRAF^{V600E} drives tumorigenesis through constitutive downstream extracellular signal-regulated kinase (ERK) activation, but high-intensity ERK activation can also trigger tumor suppression. Whether and how oncogenic ERK signaling can be intrinsically adjusted to a "just-right" level optimal for tumorigenesis remains undetermined. In this study, we found that FAK (Focal adhesion kinase) expression was reduced in *BRAF*^{V600E}-mutant adenomas/polyps in mice and patients. In *Vill-Cre;BRAF*$^{V600E/+}$;*Fak*$^{fl/fl}$ mice, *Fak* deletion maximized BRAF^{V600E}'s oncogenic activity and increased cecal tumor incidence to 100%. Mechanistically, our results showed that Fak loss, without jeopardizing BRAF^{V600E}-induced ERK pathway transcriptional output, reduced EGFR (epidermal growth factor receptor)-dependent ERK phosphorylation. Reduction in ERK phosphorylation resulted in increased mRNA expression and stability of Lgr4, promoting intestinal stemness and cecal tumor formation. Together, our findings show that a "just-right" ERK signaling optimal for *BRAF*^{V600E}-induced cecal tumor formation can be achieved via Fak loss-mediated downregulation of ERK phosphorylation.

eLife assessment

In this **important** study, the authors use a genetically engineered mouse model to reveal a tumor suppressive role for focal adhesion kinase in right-sided colon cancer. The evidence in support of the authors' claims is generally **solid**, although the data supporting the mechanism through which FAK deletion promotes tumorigenesis are **incomplete**. This work will be of interest to cancer researchers and others studying the biological consequences of tuning signal transduction pathways.

Introduction

Colorectal cancer (CRC) is a heterogeneous disease arising through several discrete evolutionary pathways. The best-known and most-studied pathway to CRC is the canonical pathway, in which cancer originates from conventional adenomatous polyps bearing *APC* (*adenomatous polyposis coli*) mutation [1,2]. Recently a new "alternative" pathway through serrated adenoma—the serrated pathway—has been uncovered. Mice studies have established that the *BRAF*^{V600E} mutation is a driver mutation in the serrated pathway [3-5]. In patients, *BRAF*^{V600E} mutation is found in 50-67% of serrated CRC [6] and 10-15% of all CRCs [7].

The "Goldilocks principle" applies to mutant *APC*-driven and mutant *BRAF*-driven intestinal tumorigenesis: a threshold of oncogenic signaling needs to be reached for dysplastic lesions to form, but optimum tumor development requires "just-right" levels of oncogenic signaling, with too much being as detrimental as too little. In the canonical pathway to CRC, the primary driving force is mutant APC-mediated activation of Wnt/β-catenin signaling [8], and the "just-right" level of Wnt/β-catenin signaling optimal for tumor formation is achieved largely by the selection for specific APC mutant proteins based on their residual β-catenin-downregulating activity [9-12]. The selection for *APC* mutations in the intestine is influenced by the underlying basal/physiological level of Wnt activity and stem-cell number, and *APC* mutation spectra vary throughout the intestinal tract resulting in different *APC* mutation spectra in the proximal and distal CRCs [10,11]. In addition to the different mutation spectra, the 'optimal' thresholds for proximal and distal cancers are also variable [11].

BRAF^{V600E} drives tumorigenesis through constitutive downstream ERK1/2 activation [13], but hyperactivation of ERK induced by oncogenic BRAF^{V600E} is not tolerated in the intestine: high ERK activation, induced by transgenic expression of oncogenic BRAF (BRAF^{V600K}) or by activation of two BRAF alleles in *BRAF*$^{V600E/V600E}$ mutant mice, engages tumor suppressive mechanisms, causing loss of stem cells and induction of differentiation and senescence [14,15]. Lowering ERK activation by treatment with ERK or MEK (mitogen-activated protein kinase kinase) inhibitor counteracted BRAF^{V600E}-induced organoid disintegration [14,16]. It is therefore presumed that maintaining ERK activation within a narrow threshold range to avoid engaging tumor suppression is pivotal for mutant BRAF to exhibit the strongest transforming activity. However, despite being highly anticipated [16], the existence of *in vivo* intrinsic fine-tuning of mutant *BRAF*-induced ERK activation has never been experimentally examined. Given that over 60 mutations have now been identified in *BRAF* [13,17], theoretically, mutation-selection could be a way to achieve optimal ERK activation. However, because the V600E mutation accounts for about 90% of BRAF mutation seen in human cancer [18], mutation-selection is not the primary means to achieve the "just-right" levels of oncogenic ERK signaling. Normally, ERK activation is self-limiting by the rapid inactivation of upstream kinases and delayed induction of dual-specific MAKP phosphatases (MKPs/DUSPs) [19]. Although feedback inhibitors of ERK signaling including DUSPs are overexpressed in BRAF^{V600E}-expressing cells, the ERK signaling pathway is refractory to upstream

feedback inhibition [20]. EGFR is a core receptor upstream of the MAPK kinase axis. *In vitro* cell culture studies show that all activating BRAF mutants are RAS-independent [21]: neither RAS inhibition [21] nor EGFR inhibition [22,23] was able to inhibit mutant-BRAF-induced ERK phosphorylation in *BRAF*-mutant human CRC cell lines.

In this study, we addressed the question that whether $BRAF^{V600E}$-induced ERK activation is still tuneable during tumorigenesis *in vivo*. If yes, what are the factors involved in the regulation? Can $BRAF^{V600E}$-induced ERK activation be fine-tuned to a "just-right" level optimal for tumor initiation? Our study identified FAK as a key regulator of $BRAF^{V600E}$-induced ERK activation in mutant *BRAF*-induced serrated tumor formation/initiation and revealed that FAK loss allows $BRAF^{V600E}$-induced ERK signaling to reach the permissive threshold "just-right" for cecal tumors to form.

Results

FAK expression is reduced in *BRAF*^{V600E}-mutant serrated lesions in humans and mice

FAK is a cytoplasmic non-receptor tyrosine kinase involved in many aspects and types of cancer [24]. To determine the role of FAK in mutant *BRAF*-induced serrated CRC, we first evaluated FAK protein expressions in human *BRAF*^{V600E}-mutated serrated tumors (11 cases). We examined tissue sections containing *BRAF*^{V600E}-mutant CRCs, sessile serrated adenoma/polyps (SSA/P)s, and adjacent histologically normal colon from the same tissue block. Results of immunohistochemistry (IHC) staining showed that FAK protein levels were lower in SSA/Ps (5/5) than in normal intestines and CRCs (5/5) (**Fig. 1a**). FAK expression was more complex in CRCs. FAK levels in CRCs were either similar to (6/11) or lower (4/11) or higher (1/11) than that of the normal intestines (**Fig. 1a, b**). FAK was mainly localized in the cytoplasm (**Fig.1b**). In mice, compared to the neighboring normal mucosa or stroma in the tumor, Fak protein levels were substantially decreased in carcinomas in the colon (**Fig. 1c**) and adenomas/polyps in the small intestine (SI) (**Fig. 1d**) in *Vill-Cre;BRAF*$^{V600E/+}$ (*BC*) mice. The downregulation of FAK in human and mouse polyps suggests that FAK loss may play a role in *BRAF*^{V600E}-induced tumor formation/initiation.

Fak deletion promotes *BRAF*^{V600E}-induced cecal tumor formation

Previous mice studies show that *Fak* deletion suppresses mammary tumorigenesis [25,26], mutant *Apc*-induced intestinal tumorigenesis [27], skin tumor formation [28], and hepatocarcinogenesis [29]. To address the functional significance of FAK downregulation in *BRAF*^{V600E}-induced serrated tumor formation/initiation, we generated the *Vill-Cre;BRAF*$^{V600E/+}$;*Fak*$^{fl/fl}$ (*FBC*) mice. The Cre-mediated recombination efficiency was confirmed by tdTomato-reporter expression in intestinal crypts in *Vill-Cre;Rosa26*$^{LSL\text{-}tdTomato/+}$ mice (**Supplementary Fig. 1a**). Deletion of Fak in the intestinal epithelium was further confirmed by IHC staining of the intestine in *FBC* mice (**Supplementary Fig. 1b**).

Similar to that seen in *BC* mice, compared to the *BRAF*$^{V600E/+}$ (*B*) mice, the *FBC* mice exhibited hyperplasia throughout the intestine (**Fig. 2a**) and thickened small and large intestines (**Supplementary Fig. 1c**). In *BC* mice, intestinal tumors were primarily developed in the small intestine at 9 months or older (**Fig. 2b**). *Fak* loss had minimal impact on tumor incidence in the small intestine and the colon, however, it greatly enhanced $BRAF^{V600E}$-induced cecal tumor formation: cecal tumor incidence increased from 0% (0/15) in 9-month or older *BC* mice to 100% (16/16) in *FBC* mice (**Fig. 2c**). Cecal adenoma/polyp started to develop in 3-month *FBC* mice and after 6 months, all mice (4/4) developed cecal tumors and 25% of the tumors (1/4) were carcinomas (**Fig. 2c, d**). At 9 months or older, 100% of the mice developed cecal tumors with a high

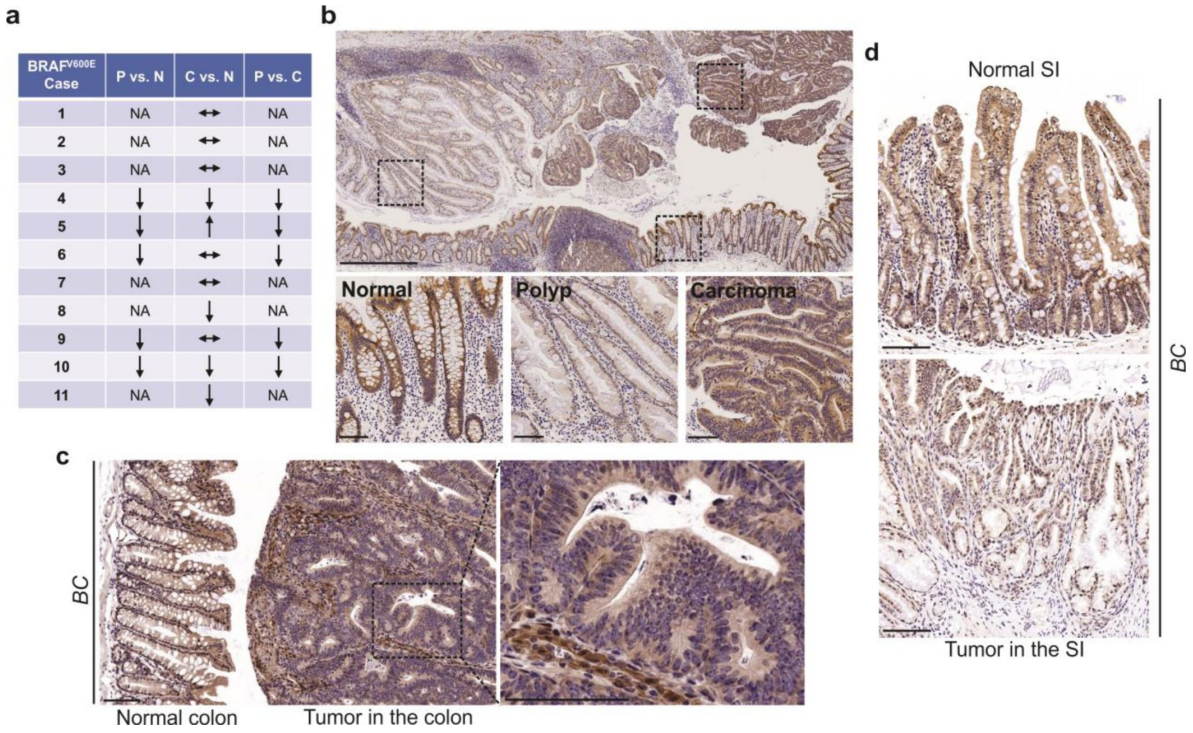

Fig. 1

FAK downregulation in serrated tumors.

a Summary of FAK IHC staining in 11 human *BRAF*^{V600E}-mutant CRC samples. N represents normal colon; P represents polyp; C represents carcinoma; NA, not applicable; ↔ represents no change; ↑ represents an increase. ↓ represents a decrease. **b** Representative IHC staining of *BRAF*^{V600E}-mutant patient SSA/P, serrated colorectal adenoma, and adjacent normal tissues. **c** IHC staining of Fak in small intestine tumors in a 12-month-old *BC* mouse. **d** Representative IHC staining of Fak in colon tumor in 12-month-old *BC* mice. Scale bars in **b**: 1 mm (upper panel) and 100 μm (lower panel). Scale bars in **c** and **d**: 100 μm.

incidence (13/16) of carcinoma (**Fig. 2c, d**, and **Supplementary Fig. 1d**). IHC staining confirmed that while the stroma showed strong Fak staining, tumor cells were Fak negative (**Fig. 2e**), hence validating that tumors were originated from Fak-deleted epithelial cells. Of note, no tumor metastasis was found in *FBC* mice. *FBC* mice were aged up to 434 days, and the life span of *FBC* mice was similar to that of BC mice.

Together, these results revealed that *Fak* deletion promotes, rather than inhibits, $BRAF^{V600E}$-induced cecal tumor formation. *BRAF*-mutant CRCs are primarily located in the right colon including the cecum [30]. The same primary tumor location suggests that the *FBC* model truthfully recapitulates human *BRAF*-mutant serrated CRCs at least by location.

The molecular feature of the cecal tumors in *FBC* mice closely resembles human SSA/Ps

To characterize the molecular signatures of the cecal tumor in *FBC* mice, we performed whole-exome sequencing on paired tumors (n=2) and neighboring mucosa. No additional driver mutations were detected in the cecal tumors (Supplementary Table 1), implying that cecal tumor formation in *FBC* mice does not require additional driver mutations. To evaluate the relevance of *FBC* cecal tumors to humans, we performed RNA-sequencing (RNA-seq) and Gene Set Enrichment Analysis (GSEA) to determine whether *FBC* cecal tumors exhibited similar gene expression signatures as human SSA/Ps [31]. The results showed that upregulated genes in human SSA/Ps were significantly enriched in cecal tumors in *FBC* mice (**Fig. 3a**). Downregulated genes in human SSA/P were also reduced in *FBC* tumors (**Fig. 3b**). Together, these results suggest that the *FBC* cecal tumors greatly resemble human serrated lesions at the molecular level.

About 50% of *BRAF*-mutated CRCs exhibit defective DNA mismatch repair [18]. The results of microsatellite instability (MSI) analysis indicated that most *FBC* cecal tumors were microsatellite stable (MSS) (**Fig. 3c**). It has been shown that mismatch repair deficiency accelerates *BRAF*-driven serrated tumorigenesis [32]. Maximizing the oncogenic activity of $BRAF^{V600E}$ without mismatch repair gene mutation and additional driver mutations suggests that in *FBC* mice, Fak loss created a “just-right” environment optimal for MSS serrated cecal tumor to form.

Fak loss increases intestinal stemness by upregulating Lgr4 levels in *FBC* mice

We explored the molecular mechanism underlying *Fak* loss-enhanced cecal tumor formation. Consistent with a prior report [27], we did not detect any abnormalities in the intestine in *Vill-Cre*; $Fak^{fl/fl}$ mice, implying that FAK loss by itself is not a driving force for intestinal tumorigenesis. A prior study showed that upon TGFβ (transforming growth factor β) receptor inactivation, $BRAF^{V600E}$-induced right-sided tumorigenesis is supported by microbial-driven inflammation [33]. To test the role of inflammation in *FBC* tumor formation, we compared sub-cryptal proprial neutrophil infiltration using myeloperoxidase (MPO) as a neutrophil marker for IHC staining. The results showed that consistent with prior findings [33], the number of MPO-positive cells was significantly higher in *BC* mice than in *B* mice, however, Fak loss did not further increase neutrophil infiltration in FBC mice (**Supplementary Fig. 2a**). Consistent with this, GSEA results showed that there was no difference in the expression of inflammatory response genes [34] in *FBC* mice and *BC* mice (**Supplementary Fig. 2b**). Together, these findings imply that Fak loss promotes tumor formation not by enhancing intestinal inflammation.

We next evaluated the roles of cellular senescence, apoptosis, cell proliferation, and *Lgr5* expression in cecal tumorigenesis in *FBC* mice. The results indicated that $BRAF^{V600E}$ was insufficient to trigger senescence evaluated by SA-β-galactosidase staining or apoptosis evaluated by the TUNEL staining in *BC* mice (**Supplementary Fig. 2c, d**). Bromodeoxyuridine (BrdU) incorporation assays confirmed mutant BRAF-induced hyperproliferation. However, Fak loss did

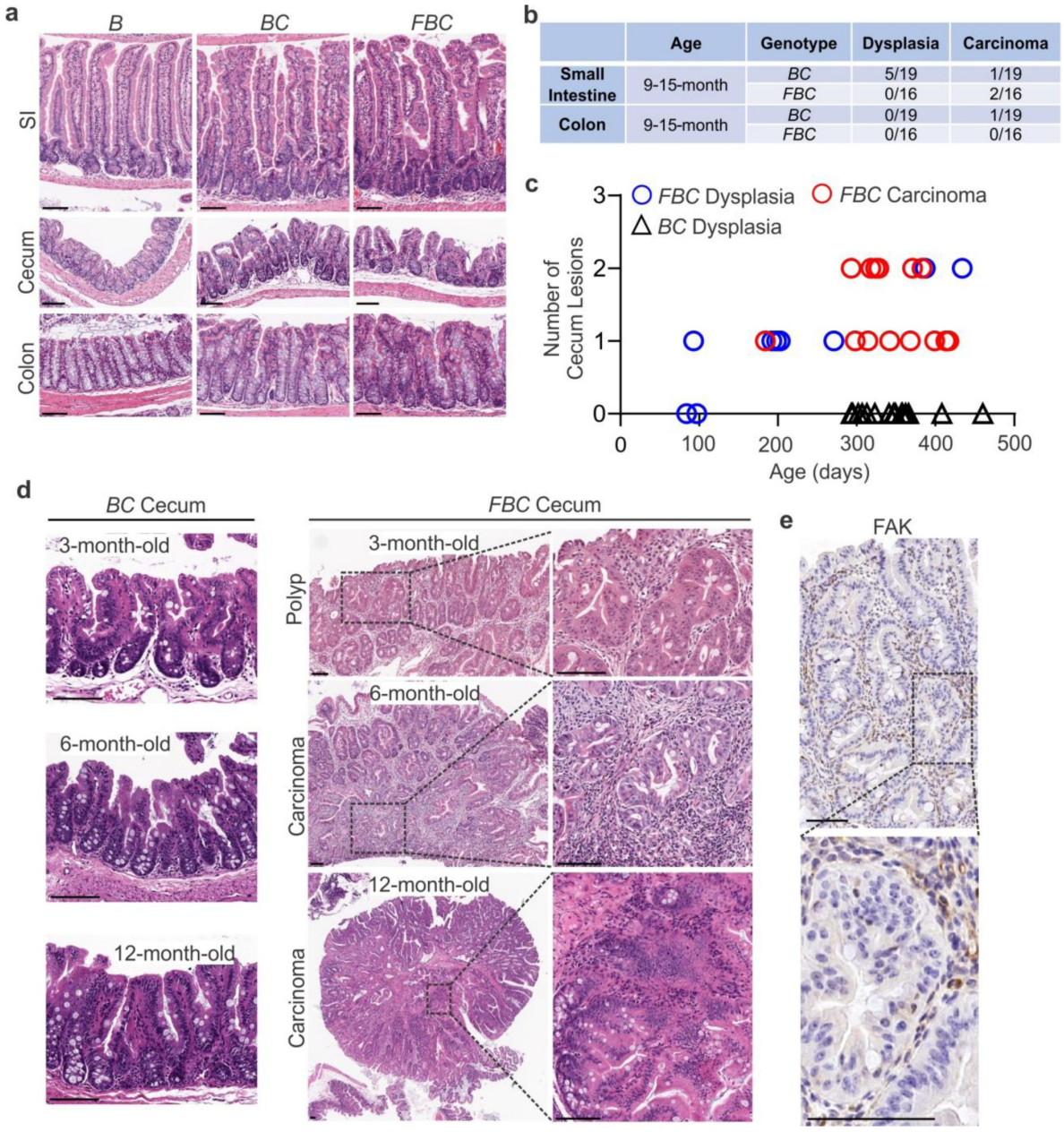

	Age	Genotype	Dysplasia	Carcinoma
Small Intestine	9-15-month	*BC*	5/19	1/19
		FBC	0/16	2/16
Colon	9-15-month	*BC*	0/19	1/19
		FBC	0/16	0/16

Fig. 2

Fak loss enhances _BRAF_^{V600E}-driven cecal tumorigenesis in mice.

a Representative hematoxylin and eosin (H&E) staining of the small intestine, cecum, and colon from indicated 6-week-old mice. **b** Summary of tumor incidence at small intestine and colon in indicted mice at the indicated age. **c** Summary of tumor incidence and tumor stage at cecum in indicated mice at the indicated age. **d** H&E staining of the cecum in *BC* mice and cecal serrated adenoma/polyp and carcinoma in *FBC* mice at the indicated age. **e** Representative IHC staining of Fak in cecal tumors in *FBC* mice. Scale bars: 100 μm.

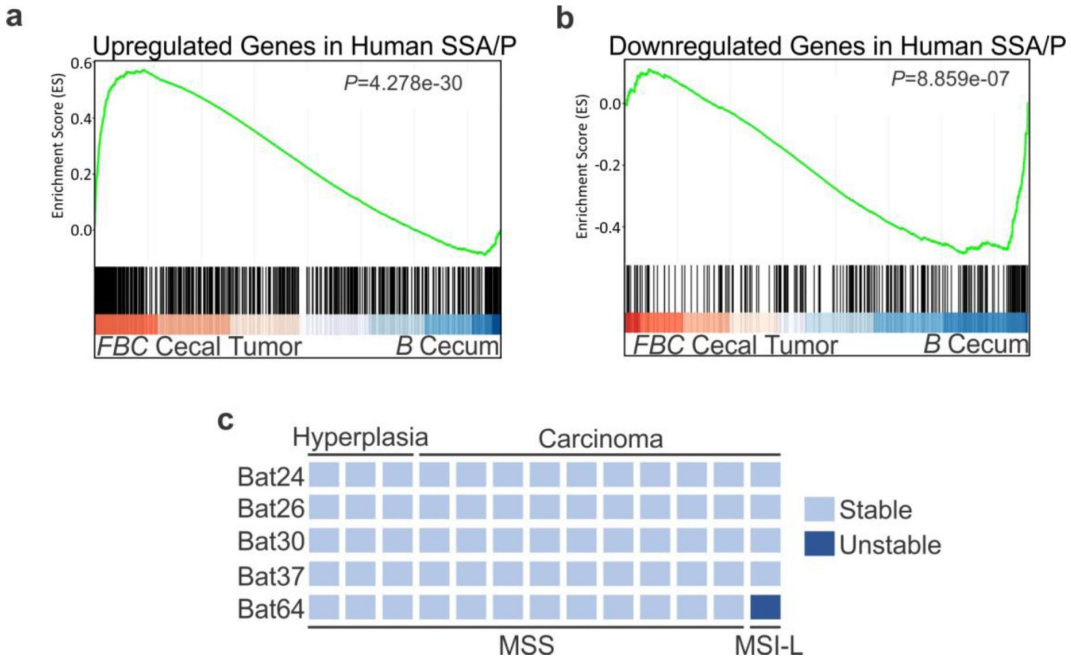

Fig. 3

Molecular characterization of cecal tumors in *FBC* mice.

a GSEA plot showing enrichment of human SSA/Ps signature genes (upregulated genes in SSA/Ps) in *FBC* cecal tumors vs normal cecal mucosa of *B* mice. **b** GSEA plot showing that downregulated genes in human SSA/Ps were also reduced in *FBC* cecal tumors. **c** Microsatellite instability status of *FBC* mice cecal mucosa and cecal carcinomas. Each column represents one sample.

not further enhance the BrdU incorporation rate (**Supplementary Fig. 2e**). These results indicated that *Fak* deletion promotes tumor formation not through modulating cellular senescence, apoptosis, and cell proliferation.

Given that $BRAF^{V600E}$ drives tumorigenesis through constitutive downstream ERK1/2 activation [13], we examined the impact of Fak loss on ERK pathway transcriptional output. GSEA analysis showed that ERK pathway output was significantly increased in *BC* mice (**Fig. 4a**), which was consistent with the earlier report [20], but Fak loss did not further enhance it (**Fig. 4f**). Wnt pathway activation [32] and activation of transcription co-factor YAP have been implied in $BRAF^{V600E}$-induced serrated tumorigenesis [33]. In this study, our GSEA results also showed that the expression of intestinal Wnt signature genes [35] and YAP target genes [36] were significantly higher in *BC* mice than in *B* mice (**Fig. 2b, c**), again, Fak loss did not further enhance the activations (**Fig. 2g, h**). Together, these findings excluded the possibility that Fak loss promotes cecal tumor formation through enhancing ERK pathway output and activation of the Wnt pathway and the YAP pathway.

In mice, $BRAF^{V600E}$ poorly initiates colon cancer due to oncogenic BRAF-induced tissue differentiation and loss of intestinal stem cells [15]. Consistent with this, GSEA results showed increased expressions of intestinal differentiation signature genes [37] (**Fig. 4d**) and decreased expressions of intestinal stem cell signature genes [38] (**Fig. 4e**) in *BC* mice. Fak deletion did not reverse $BRAF^{V600E}$-induced tissue differentiation (**Fig. 4i**) but significantly enhanced intestinal stemness (**Fig. 4j**). These results revealed that Fak deletion promotes $BRAF^{V600E}$-induced cecal tumor formation through increasing intestinal stemness.

The adult stem cell marker Lgr5 and its relative Lgr4 are R-spondin receptors mediating R-spondin signaling and are critical for intestinal stemness [39,40]. Mutant BRAF reduces *Lgr5* expression in the intestinal crypt [15,33]. Our results confirmed the downregulation of *Lgr5* in the cecum crypt in *BC* mice, and we found that Fak loss did not restore *Lgr5* expression in *FBC* mice (**Supplementary Fig. 2f**). These results thus excluded the possibility that Lgr5 mediates Fak loss-induced intestinal stemness.

Prior studies show that the fetal type of intestinal stem cells has a strikingly different transcriptome than that of adult intestinal stem cells and the receptor LGR4, but not LGR5, is essential for the cells [41]. In $VillinCre^{ER}$;$Braf^{LSL\text{-}V600E/+}$;$Alk5^{fl/fl}$ mice, the proximal colonic tumors exhibit fetal intestinal signature [33]. Consistent with the notion that mutant *BRAF*-driven right-sided colonic tumors are fetal progenitor phenotypes, GSEA results confirmed enrichment of the fetal-type transcriptomic signatures [41] in cecal mucosa in *BC* mice, and the fetal signature was further enriched in *FBC* mice (**Fig. 4k**). Accordingly, the immunoblotting analysis showed that the protein level of Lgr4 was increased in the intestine epithelium in *FBC* mice (**Fig. 4i**). Consistent with the fact that intestinal *Lgr5* expression was low in *FBC* mice (**Supplementary Fig.2f**), *FBC* tumors mainly expressed *Lgr4* but not *Lgr5*, whereas *BC* tumors and $Apc^{min/+}$ tumors expressed both *Lgr5* and *Lgr4* (**Fig. 4m**). These results suggest that in *FBC* mice upregulated Lgr4 mediated the intestinal stemness increase.

FAK loss downregulates EGFR-dependent ERK phosphorylation to increase Lgr4 mRNA expression and stability

We addressed how Fak loss mediates Lgr4 increase. A prior study suggested that Wnt signaling maintains quiescent intestinal stem cell pools through suppression of the MAPK pathway in the intestine [42]. Given the fact that Fak loss did not jeopardize ERK pathway transcriptional output (**Fig. 4f**), Fak loss may increase intestinal stemness by inhibiting ERK phosphorylation. To test, we first compared the levels of phosphorylated ERK across the intestines in *B* mice, *BC* mice, and *FBC* mice. As anticipated, $BRAF^{V600E}$ increased p-ERK levels throughout the intestine (**Fig. 5a**). FAK is known to be positively involved in ERK1/2 activation [24]. Consistent with this, in *FBC* mice,

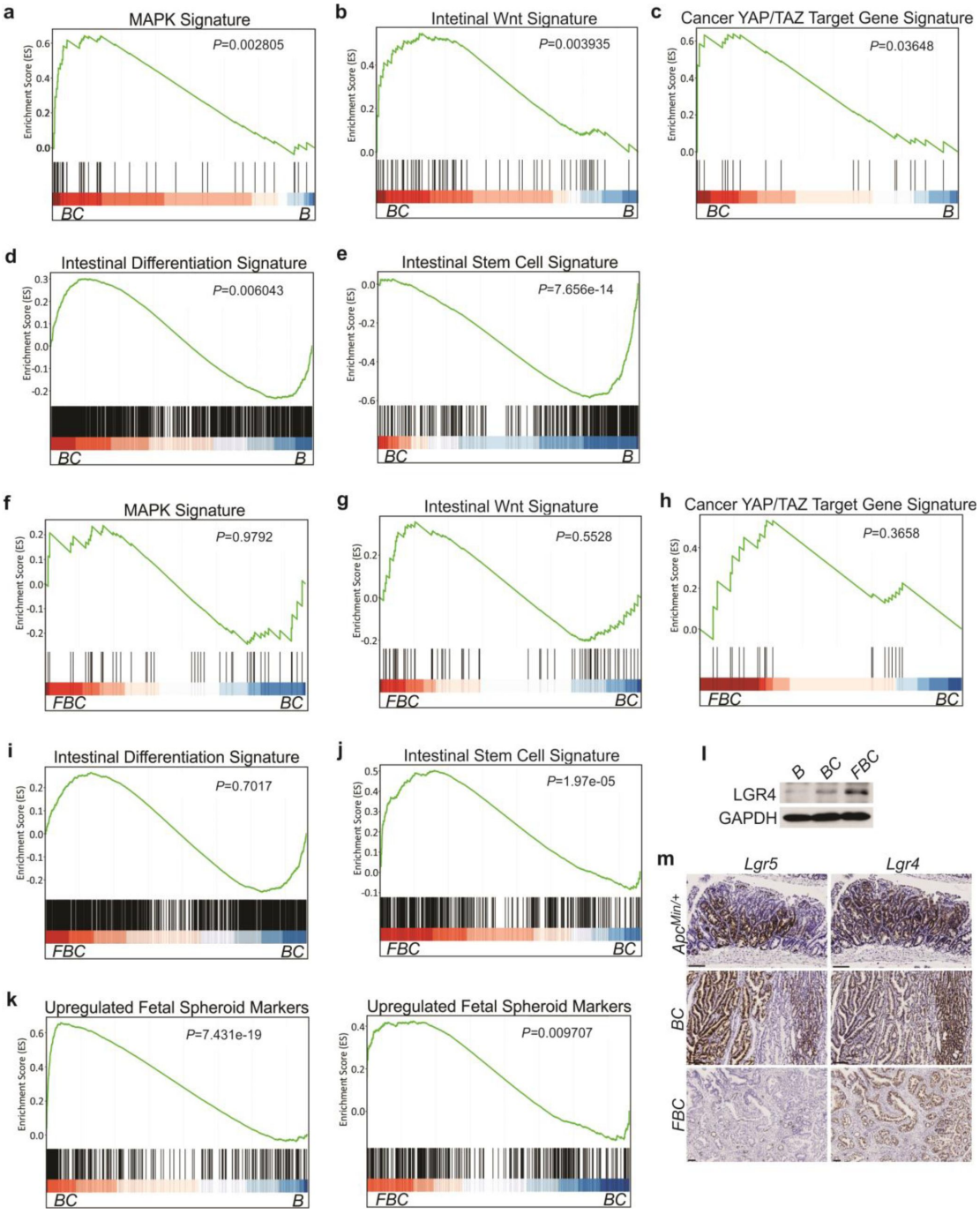

Fig. 4

BRAF^{V600E} mutation and *Fak* loss-mediated changes in signaling pathways.

GSEA analysis showing upregulation of MAPK signature (**a**), intestinal WNT signaling (**b**), YAP/TAZ target gene signature (**c**) and intestinal differentiation signature (**d**), and downregulation of intestinal stem cell signature (**e**) in the cecum of *BC* mice vs *B* mice (n=4 per group). GSEA plots revealed no significant change in MAPK signature (**f**), intestinal WNT signaling (**g**), YAP/TAZ target gene signature (**h**), and intestinal differentiation signature (**i**) in the cecum of *FBC* mice vs *BC* mice, but enrichment of stem cell signature in *FBC* mice (**j**) (n=4 per group). **k** GSEA analysis showing upregulation of upregulated fetal spheroid markers in the cecum of *BC* mice vs *B* mice, and further enrichment in the cecum of *FBC* mice vs *BC* mice (n=4 per group). **l** Immunoblotting analysis of LGR4 in the cecum from indicated 6-week-old mice. **m** Representative in situ hybridization (ISH) staining of tumor sections from *Apc*$^{Min/+}$, *BC*, and *FBC* mice using *Lgr4* and *Lgr5* probes. Scale bars: 100 μm.

FAK deletion suppressed mutant BRAF-induced elevation of p-ERK (**Fig. 5a**). The decoupling of ERK pathway output (no change) and the level of p-ERK (reduced) upon Fak loss is in line with a prior report suggesting that the level of ERK phosphorylation does not truthfully reflect ERK pathway activation [20].

We next examined how Fak loss altered $BRAF^{V600E}$-induced phosphorylation of ERK. A prior study found that FAK promotes EGFR signaling [43], raising the possibility that FAK regulates ERK phosphorylation through EGFR. We then evaluated Egfr activation (represented by phosphorylated EGFR at tyrosine 1068) in the mice. The results showed that the level of phosphorylated $Egfr^{Y1068}$ was increased in *BC* mice throughout the intestine (**Fig. 5b**). In *FBC* mice, Fak deletion moderately reduced $BRAF^{V600E}$-induced Egfr activation (**Fig. 5b**) and suppressed Egfr downstream signal transduction as evidenced by the decreased levels of phosphorylated c-Raf^{S338} and $MEK1/2^{S217/221}$ in *FBC* mice (**Supplementary Fig. 3a**). To validate that EGFR indeed regulates $BRAF^{V600E}$-induced ERK phosphorylation, we treated *BC* mice with the EGFR inhibitor erlotinib. Erlotinib treatment, without significantly reducing ERK pathway output (**Supplementary Fig. 3b**), indeed suppressed phosphorylation of C-RAF, MEK, and ERK (**Fig. 5c**). Of note, Fak deletion had no impact on the level of p-EGFR and p-ERK in control mice (**Supplementary Fig. 3c**). Inhibition of Fak kinase activity by FAK inhibitor PF-562271 did not affect the phosphorylation of Egfr and ERK (**Fig. 5d**), implying that the kinase activity of Fak is not involved in the FAK/EGFR/ERK regulation in $BRAF^{V600E}$-induced serrated tumorigenesis.

FAK complexes with activated EGFR to promote EGFR signaling [43]. We assessed whether FAK interacts with EGFR in $BRAF^{V600E}$-mutant cells. The results of co-immunoprecipitation using lysates from cecal mucosa confirmed the Fak-Egfr interaction and revealed that the Fak-Egfr interaction was increased in *BC* mice and inhibition of Egfr appeared not to affect the Fak-Egfr binding (**Supplementary Fig. 3d**). ERK phosphorylation is refractory to EGFR inhibition in human $BRAF^{V600E}$-mutant CRC cell lines [22,23], however, the FAK-EGFR interaction was still detected in HT29 CRC cells and the interaction was not affected by either EGFR inhibition or FAK inhibition (**Supplementary Fig. 3e**). These results indicated that FAK/EGFR interaction alone is not sufficient for FAK getting involved in the regulation of MAPK signaling.

The contradictory results seen in *BC* mice and human $BRAF^{V600E}$-mutant CRC cell lines could result from the differences between *in vitro* culture systems and *in vivo*. To test, we examined whether inhibition of Egfr leads to ERK inhibition in freshly isolated cecal crypts from *BC* mice and *BC* cecal organoids. The results showed that inhibition of Egfr did not reduce ERK phosphorylation, confirming that the contradictory findings resulted from *in vitro* and *in vivo*. We speculate that the lack of certain stromal factors *in vitro* is responsible for the EGFR's inability to transmit its signal to activate ERK.

Finally, we examined whether and how a reduction in ERK phosphorylation increases Lgr4 expression/stemness. Our results showed that treatment with MEK inhibitor increased the mRNA expression of LGR4 in human $BRAF^{V600E}$-mutant CRC HT29 cells (**Fig 5f**) and *BC* mice (**Fig. 5g**), uncovering a negative association between the level of ERK phosphorylation and mRNA expression of Lgr4. Of note, inhibition of ERK activation in *BC* mice was confirmed by the abrogation of ERK phosphorylation (**Fig 5g**) and suppression of ERK pathway transcriptional output (**Supplementary Fig. 4**). This negative association was further supported by our observation that the mRNA levels of Lgr4 were higher, albeit not statistically significant, in *FBC* mice than in *BC* mice (**Fig 5h**). Regulation of Lgr4 protein stability represents an important mechanism of modulating Lgr4 function [44]. Our cycloheximide chase analysis results showed that inhibition of ERK phosphorylation by MEK inhibitor treatment dramatically enhanced Lgr4 protein stability in $BRAF^{V600E}$-mutant CRC cell line HT29 cells (**Fig 5i**). This finding revealed the inverse correlation between the level of ERK phosphorylation and the protein stability of Lgr4.

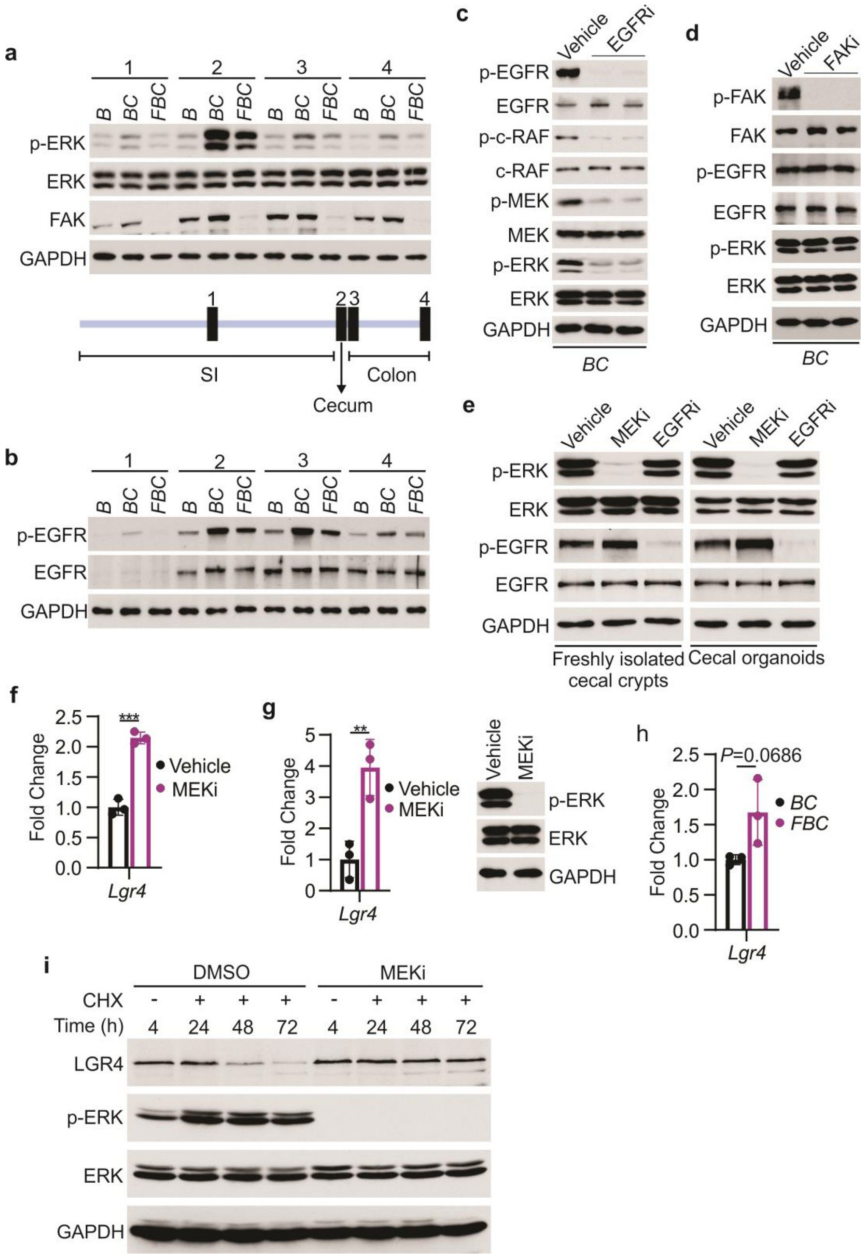

Fig. 5

Fak loss inhibits ERK phosphorylation and upregulates Lgr4.

a and **b** Immunoblotting analysis of intestinal mucosa lysates from indicated bowel subsites in indicated 6-week-old mice. **c** Immunoblotting analysis of cecum lysates from 6-week-old *BC* mice treated with vehicle or EGFR inhibitor erlotinib for 4 hours. Each lane represented a single mouse. **d** Immunoblotting analysis of cecum lysates from 6-week-old *BC* mice treated with vehicle or FAK inhibitor PF-562271 for 4 hours. Each lane represented a single mouse. **e** Immunoblotting analysis of lysates from freshly isolated cecal crypts and cecal organoids treated with DMSO, MEK inhibitor PD0325901, or erlotinib, respectively as described in Method. **f** qRT-PCR of *Lgr4* using lysates from HT-29 cells treated with the vehicle and MEKi for 4 hours. Data presented as mean ± SD (***P<0.001; Student's t-test, two-tailed). **g** qRT-PCR of *Lgr4* using cecum lysates from *BC* mice treated with vehicle or MEKi for 6 hours. Data presented as mean ± SD (**P<0.01; Student's t-test, two-tailed). Abrogation of ERK phosphorylation at T202/Y204 in the cecum was confirmed by western blot. **h** qRT-PCR of *Lgr4* in cecum from *BC* and *FBC* mice (n=3 per group). Data presented as mean ± SD (P value calculated using two-tailed Student's t-test). **i** Immunoblotting analysis of the lysates from HT-29 cells treated with cycloheximide (100 μg/ml) and/or MEK inhibitor PD0325901 (10 μM) as indicated.

Together, these results suggest that Fak loss lowers $BRAF^{V600E}$-induced ERK phosphorylation to increase Lgr4 mRNA expression and protein stability, thereby enhancing intestinal stemness and cecal tumor formation.

FAK's influence on oncogenic MAPK-driven intestinal tumorigenesis depends on FAK's impact on ERK phosphorylation

Fak loss reduced ERK phosphorylation in *FBC* mice (**Fig. 5a**) but not in control mice with wild-type *BRAF* (**Supplementary Fig. 3c**). To determine whether FAK is involved in other oncogenic MAPK-driven tumors, we generated *Vill-Cre;Kras*$^{LSL\text{-}G12D/+}$ (*KC*) mice and *Vill-Cre;Kras*$^{LSL\text{-}G12D/+}$;*Fak*$^{fl/fl}$ (*FKC*) mice. In *KC* mice, the endogenous expression of oncogenic Kras induces serrated hyperplasia, however, high ERK activation-induced senescence prevents hyperplasia progression into dysplasia [45]. As shown in **Fig. 6a**, no tumor was found in *KC* mice (n=6, 9-months-old) and *FKC* mice (3-month-old, n=3; 6-month-old, n=3; 9-month-old, n=4). Immunoblotting results confirmed that Fak loss failed to influence the phosphorylation of Egfr or ERK (**Fig. 6b**). The co-immunoprecipitation results showed that Fak complexed with Egfr in *KC* mice similarly as in *BC* mice (**Fig.6c**), implying that the noninvolvement of Fak was not due to the lack of Fak/Egfr interaction. A recent preprint (*https://doi.org/10.1101/2020.07.02.185173*) suggests that "EGFR network oncogenesis cooperates with weak oncogenes in the MAPK pathway", which inspired us to propose the notion that EGFR participates in the regulation of ERK phosphorylation only when the p-ERK level is relatively low. In *KC* mice, $KRAS^{G12D}$ induces extremely high levels of ERK phosphorylation, high enough to cause intestinal senescence [45]. Given the level of increased p-ERK in *KC* mice, one would expect that ERK phosphorylation is EGFR-independent. The EGFR independence was confirmed by our results showing that pharmacologic abrogation of EGFR activation had no impact on $KRAS^{G12D}$-induced ERK phosphorylation in *KC* mice (**Fig 6d**). Our notion was further supported by clinical findings. Anti-EGFR therapy is excluded for patients with *KRAS*-mutant CRC, supporting that EGFR has minimum impact on downstream MAPK signaling upon *KRAS* mutation. However, when ERK activation is inhibited by $KRAS^{G12C}$ inhibitors, EGFR signaling acts as the dominant mechanism of colorectal cancer resistance to $KRAS^{G12C}$ inhibitors [46].

To address whether FAK downregulation is specific to human *BRAF*-mutant CRCs, we compared FAK expression levels in CRCs with different driver mutations using the TCGA database. TCGA analysis revealed that *FAK* mRNA levels were significantly lower in *BRAF*-mutated CRCs than in *APC*-mutated CRCs or *KRAS*-mutant CRCs (**Fig. 6e**). This result is consistent with the result seen in mice, again, it suggests that FAK is not involved in the regulation of *KRAS*-mutant CRCs.

In mice, mutant BRAF-induced ERK activation is cancer stage-dependent with significantly higher levels of phosphorylated ERK in high-grade dysplasia and carcinoma [3], suggesting that different tumor stages may require different levels of p-ERK. If FAK is a key regulator of ERK phosphorylation in mutant *BRAF*-induced serrated tumorigenesis in patients, one would expect the level of FAK may increase as the tumors progress. Consistent with this notion, we observed that FAK levels were higher in BRAF-mutant CRCs than in BRAF-mutant polyps (**Fig 1a**), TCGA analysis (**Fig. 6e**) further confirmed that FAK expression was restored to a level similar to normal intestines, albeit still significantly lower than in APC mutant or KRAS mutant CRCs (**Fig. 6e**).

In patients, BRAF mutations are divided into two groups: Activator and amplifier mutation [47]. In CRC, the majority (80%-90%) of activating mutations in BRAF are V600E [18]. Among these mutants, based on their kinase activities, $BRAF^{V600E}$ belongs to the high-activity mutants, and the rest of the mutants except G595R (with impaired BRAF kinase activity *in vitro* but still induce constitutive ERK activation *in vivo*,) are intermediate activity mutants [48]. If mutant BRAF-induced ERK phosphorylation needs to reach a "just-right" level via FAK downregulation in patients, one would expect that the degree of FAK downregulation is BRAF mutant activity-

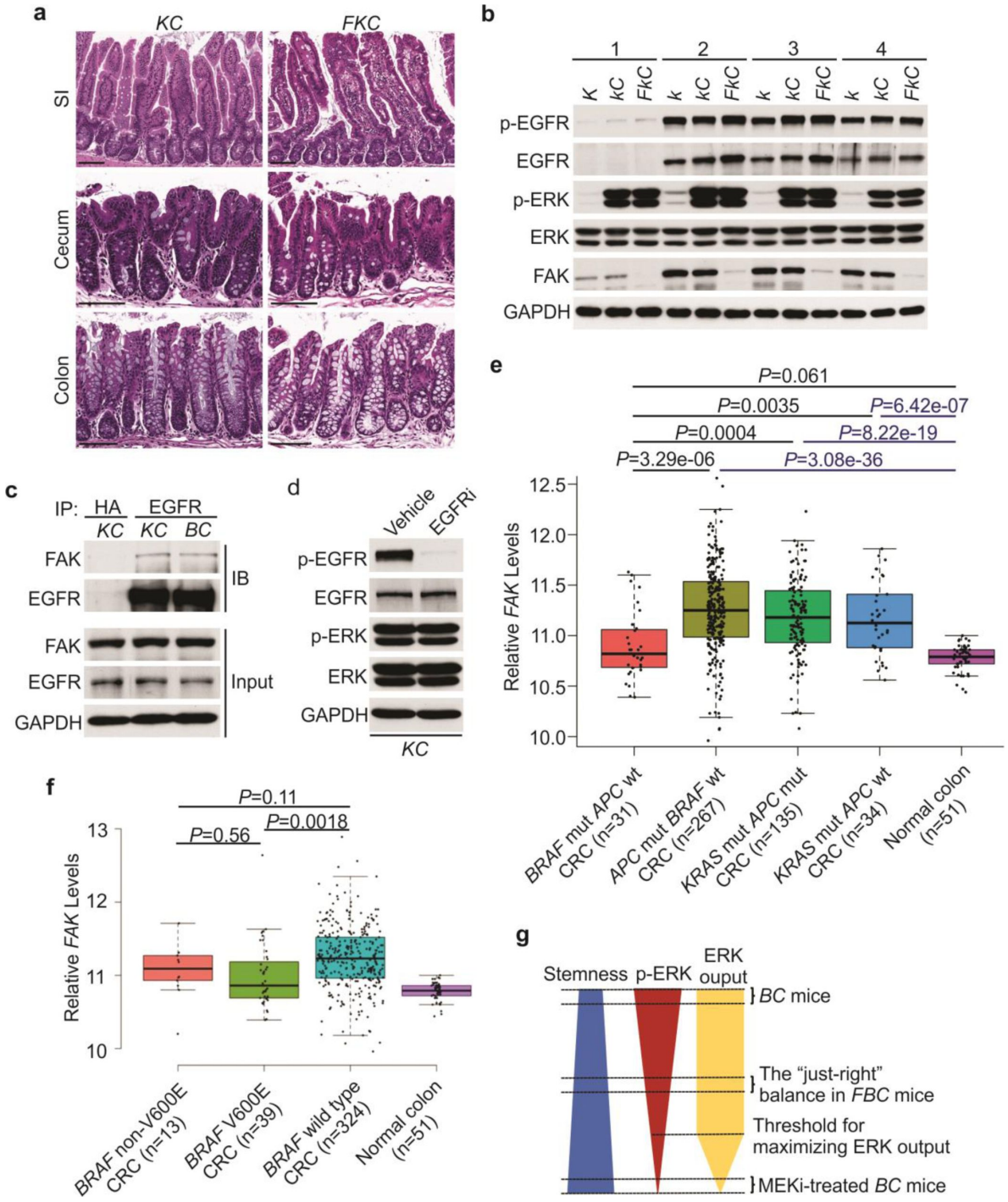

Fig. 6

ERK activation is FAK/EGFR-independent in *KC* mice.

Representative hematoxylin and eosin (H&E) staining of the small intestine, cecum, and colon from indicated 9-month-old mice. **b** Immunoblotting analysis of intestinal mucosa lysates from indicated bowel subsites in indicated 6-week-old mice. **c** The cecal mucosa lysates from 6-week-old *KC* and *BC* mice were used for immunoprecipitation and immunoblotting with the indicated antibodies. **d** Immunoblotting analysis of cecum lysates from 6-week-old *KC* mice treated with vehicle or EGFR inhibitor erlotinib for 4 hours. **e** and **f** Comparison of *FAK* expression levels between CRCs with indicated mutations by analysis of TCGA RNA-sequencing dataset. Data were analyzed for statistical significance using a Student t-test. **g** Diagram of the "just-right" MAPK signaling model in the serrated pathway.

dependent, and there could be a correlation between the activity of BRAF mutants and the degree of FAK reduction. Consistent with this speculation, TCGA data analysis confirmed that CRCs with *BRAF*^{V600E} mutation had lower FAK expression than CRCs with non-V600E mutations and *BRAF* wild-type CRCs (**Fig. 6f**). Although the differences between V600E and non-V600E groups were not statistically significant due to limited sample numbers, they might be biologically relevant.

Discussion

The current study finds that in *BRAF*^{V600E}-mutant intestinal epithelium, elevating the p-ERK level to a minimum threshold is sufficient to maximize the pathway transcriptional output, i.e., only lowering the p-ERK level below the threshold will significantly abrogate the ERK pathway transcriptional output. Due to the negative association between ERK phosphorylation and intestinal stemness, any increase in ERK phosphorylation will decrease intestinal stemness (**Fig 6g**). In *BRAF*^{V600E}-mutant intestinal epithelium, ERK phosphorylation is EGFR/RAS/c-RAF-dependent. The involvement of EGFR provides an opportunity for non-MAPK pathway factors such as FAK to participate in the regulation of ERK phosphorylation to influence the biological outcomes of *BRAF* mutation. This study has established the first "just-right" MAPK signaling model of BRAF^{V600E}-induced tumor formation (**Fig. 6g**). Our results show that by lowering BRAF^{V600E}-induced ERK phosphorylation, Fak loss, without jeopardizing the ERK pathway transcriptional output, enhances mRNA expression and protein stability of Lgr4, thereby increasing intestinal stemness and promoting cecal tumor formation in mice.

High-level activation of oncogenes (e.g. KRAS, BRAF, and c-MYC) triggers intrinsic tumor suppression [45,49-52]. Genetic abrogation of tumor suppressors such as p53 or p16 revokes the tumor-suppressive barrier thereby facilitating oncogene-induced tumorigenesis [4,45,50,51]. Cooperation with other oncogenic stimulation, such as co-expression of c-MYC and KRAS, ultraviolet radiation on melanocytes expressing BRAF^{V600E}, can also break the suppressive barrier [53,54]. In cellular models [55,56], overexpression of MKP/DUSPs evades high ERK activation-induced tumor suppression. Whether and how the suppressive barrier can be avoided or reduced *in vivo* has never been experimentally tested. The current study is the first demonstration that mutant BRAF-induced activation of ERK signaling is tuneable *in vivo* and by tuning ERK activation to alter the suppressive barrier, FAK regulates BRAF transforming activity.

In *BRAF*-mutated melanoma, a complete shutdown of the MAPK pathway is necessary for significant tumor response [57]. In patients with *BRAF*^{V600E}-mutated CRCs, a combination of encorafenib, cetuximab, and binimetinib (MEK inhibitor) treatment increased the response rate to 26% [58], highlighting the importance of complete ERK pathway inhibition. However, the inverse correlation between the level of phosphorylated ERK and the level of stemness/Lgr4 expression seen in mutant BRAF expressing intestinal epithelial cells let us speculate that inhibition of ERK phosphorylation may cause stemness increases in *BRAF*-mutated CRC cells. The molecular mechanisms underlying ERK phosphorylation inhibition-mediated stemness increase remain to be determined. Given the importance of cancer cell stemness in treatment resistance [59], we propose that the optimal treatment outcome can only be achieved when the inhibition of ERK phosphorylation-mediated stemness increase is simultaneously suppressed.

In sum, the current study reveals the existence of a balance—between the level of phosphorylated ERK, the level of ERK pathway output, and the level of intestinal stemness. Our results show that the "just-right" balance optimal for *BRAF*^{V600E}-induced cecal tumor formation can be achieved through FAK alteration. Achieving optimal treatment response in *BRAF*-mutated CRC patients, though, may require abrogation of the p-ERK-stemness regulatory link. That said, the current study could have profound implications for the development of new anticancer agents and new treatment approaches for patients with *BRAF*-mutated CRC.

Methods

Mice and Treatment

All animal procedures were performed according to protocols approved by the Institutional Animal Care and Use Committee at the University of Pittsburgh. Mice were fed a standard diet (diet ID 5P75; Purina LabDiet, St. Louis, MO). *Fak*$^{fl/fl}$ mice were received from the Mutant Mouse Resource & Research Centers (MMRRC, cat. no. 009967-UCD). *Villin-Cre* (cat. no. 021504), *Braf*$^{LSL-V600E/+}$ (cat. no. 017837), *Kras*$^{LSL-G12D/+}$ (cat. no. 008179) and *Rosa26-tdTomato* (cat. no. 007914) mice were obtained from the Jackson Laboratory. Genotyping was performed according to the protocols provided by MMRRC and the Jackson Laboratory. *Villin-Cre* and *Braf*$^{LSL-V600E/+}$ mice were crossed to get the *BC* mice. The littermates harboring *Braf*$^{LSL-V600E}$ allele were used as controls whenever available. To get the *FBC* mice, *Fak*$^{fl/fl}$ mice were first crossed with *Villin-Cre* mice and *Braf*$^{LSL-V600E/+}$ mice, respectively. The offspring *Villin-Cre;Fak*$^{fl/+}$ and *Braf*$^{LSL-V600E/+}$*;Fak*$^{fl/+}$ mice were further crossed with *Fak*$^{fl/fl}$ mice to get the *Villin-Cre;Fak*$^{fl/fl}$ (*FC*) and *Braf*$^{LSL-V600E/+}$*;Fak*$^{fl/fl}$ (*FB*) mice. The *FBC* mice were finally obtained by crossing *FC* and *FB* mice. Same strategy was used to generate the *FKC* mice. *BC, FBC, KC* and *FKC* mice were euthanized at the indicated age to evaluate the tumor formation. *Villin-Cre* mice and *Rosa26*$^{LSL-tdTomato/LSL-tdTomato}$ mice were crossed to get the *Villin-Cre*; *Rosa26*$^{LSL-tdTomato/+}$ mice.

For Bromodeoxyuridine (BrdU) labeling, six-week-old mice were given BrdU (MilliporeSigma) at a dose of 100 mg/kg by intraperitoneal injection two hours before harvesting. For inhibitor treatment, six-week-old mice were given vehicle (a mixture of 50% DMSO and 50% PEG 400), PF-562271 (60 mg/kg in the vehicle), or Erlotinib (100 mg/kg in vehicle) by a single oral gavage four hours (for immunoblotting) or six hours (for qRT-PCR analysis of ERK output genes) before harvesting. MEK inhibitor PD0325901 was given to mice by a single oral gavage at a dose of 25 mg/kg in the vehicle six hours before harvesting. All experiments were performed in both male and female mice.

Cell culture and treatment

HT-29 cells were obtained from the American Type Culture Collection (ATCC) and cultured in DMEM supplemented with 5% fetal bovine serum, 100 units/ml penicillin, and 100 µg/ml streptomycin, in a 37°C humidified incubator containing 5% CO_2. The cells were treated with DMSO, PF-562271 (5 µM), or erlotinib (10 µM) for one hour before being harvested for immunoprecipitation.

Protein stability assay

HT-29 cells were seeded twenty-four hours before the experiments. The cells were treated with 100 µg/ml cycloheximide (Selleck Chemicals), 10 µM MEK inhibitor PD0325901, or their combination as indicated. Then the cells were harvested, and the whole cell lysates were used for immunoblotting.

Organoid culture and treatment

Mouse organoids were isolated according to the published protocol with some modifications [60]. Briefly, the cecum of the *BC* mouse was rinsed with cold PBS, cut into small pieces, and washed eight times in cold PBS by gently pipetting. The fragments were incubated in 10 mM EDTA diluted in PBS for 8 minutes in a 37 °C tube rocker. Then the EDTA solution was removed and the tissue was pipetted 10 times in cold PBS. The supernatant was collected and centrifuged at 300 × g for 3 minutes at 4 °C. The cell pellet was washed with DMEM/F-12 medium and centrifuged at 400 × g for 3 minutes at 4 °C. The pellet was resuspended in Cultrex Reduced Growth Factor Basement Membrane Extract, Type R1 (R&D Systems), and seeded into a 24-well plate. Organoids were cultured using Mouse IntestiCult™ Organoid Growth Medium (STEMCELL Technologies) in a 37°C

humidified incubator containing 5% CO_2. The medium was changed every other day. For inhibitor experiments, the freshly isolated crypts (one hour after seeding) and organoids (five days after seeding) were treated with 10 μM EGFR inhibitor erlotinib and 10 μM MEK inhibitor PD0325901, respectively, for two hours. To isolate protein for immunoblotting after treatment, the crypt cultures were scraped and suspended in 500 μl of TrypLE Express containing 10 μM EGFR inhibitor or 10 μM MEK inhibitor and incubated at a 37°C water bath for 5 minutes with occasional agitation. After the addition of 500 μl of DMEM/F-12 medium, the crypt cultures were centrifuged at 400 × g for 3 minutes at 4 °C. The cell pellets were resuspended in cold PBS and centrifuged again. The final pellets were lysed in RIPA buffer (Alfa Aesar) supplemented with protease inhibitor and phosphatase inhibitor (Thermo Fisher Scientific). Crypt cultures treated with DMSO were used as controls. The lysates were quantified and resolved by sodium dodecyl sulfate-polyacrylamide gel electrophoresis (SDS-PAGE) and blotted with the indicated antibodies.

Immunoblotting and immunoprecipitation

After the mice were euthanized, the entire intestines were immediately removed and rinsed twice with ice-cold PBS. The mucosal layers of the small intestine (about 1 cm length), colon (about 1 cm length), and cecum (entire cecum, without appendix) were harvested by scraping with a blade and all procedures were performed on ice. The freshly collected tissue was lysed in RIPA buffer supplemented with protease inhibitor and phosphatase inhibitor. The lysates were quantified and resolved by SDS-PAGE and blotted with the indicated antibodies. SuperSignal Western Blot Enhancer (Thermo Fisher Scientific) was used to enhance the blotting signal when needed. To detect the interaction between FAK and EGFR, the tissue lysates were pre-cleared with Protein G-sepharose beads at 4°C for 30 min. The cleared lysates were incubated with anti-EGFR antibody conjugated to agarose (Santa Cruz Biotechnology) or EZview Red anti-HA affinity gel (MilloporeSigma) at 4°C for 4 hr. The immunoprecipitates were washed three times with lysis buffer containing 20 mM Tris-HCl, pH 7.5, 150 mM NaCl, 1 mM EDTA, 1% NP40, and 10% Glycerol, and subjected to SDS-PAGE followed by immunoblotting. The antibodies used for immunoblotting are shown in Supplementary Table 2. All experiments were independently repeated at least three times.

Immunohistochemistry, in situ hybridization, BrdU staining, TUNEL staining, and histopathology

The de-identified human colon tissue samples from *BRAF*^{V600E}-mutated CRC patients were provided by the University of Pittsburgh School of Medicine, Department of Pathology tissue core. For mouse tissue sections, the mouse intestine was dissected out, rinsed twice with ice-cold PBS, fixed overnight in 10% neutral buffered formalin at 4°C, embedded in paraffin, and finally cut into 5-μm sections. The sections were deparaffinized in xylenes and rehydrated in graded alcohol solutions followed by washes in distilled water. Antigen retrieval was performed for 15 minutes in boiling pH 8 EDTA buffer (Abcam). The sections were allowed to cool to room temperature and then washed with PBS. The endogenous peroxidase was blocked with 3% hydrogen peroxide for 10 minutes. After washing with PBS, the sections were blocked with 20% goat serum diluted in PBS for 45 minutes. Sections then were incubated overnight at 4°C in a humidified chamber with primary antibodies diluted in 3% BSA. Primary antibodies used in this study are listed in Supplementary Table 2. The sections were washed with PBS and incubated with secondary antibodies for 1 hour at room temperature. Color visualization was performed with 3.3'-diaminobenzidine until the brown color fully developed. The sections were counterstained with hematoxylin, dehydrated, and coverslippped with permanent mounting media. The slides were scanned using the Aperio digital pathology slide scanner (Leica Biosystems). The images were analyzed using Aperio ImageScope software.

In situ hybridization (ISH) was performed using the RNAscope 2.5 HD Reagent Kit-BROWN (Advanced Cell Diagnostics) according to the manufacturer's instructions. The following probes from Advanced Cell Diagnostics were used: *Lgr5* (cat. no. 312171) and *Lgr4* (cat. no. 318321).

BrdU staining was performed on formalin fixed paraffin embedded (FFPE) tissue sections using monoclonal anti-BrdU antibody (MilloporeSigma) as described by the manufacturer. For Terminal deoxynucleotidyl transferase dUTP nick-end labelling (TUNEL) staining, the FFPE tissue sections was deparaffinized, treated with proteinase K and labelled using the In Site Cell Death Death Detection Kit POD (MilloporeSigma) according to the manufacturer's instructions. To quantify the results of BrdU, TUNEL and RFP staining, thirty crypts/villi per mouse were scored for three mice in each group.

Myeloperoxidase (MPO) was used as the marker for neutrophils. Ten random-chosen 500 μm-length cecum sections were evaluated for each mouse. MPO^+ cells within the band of lamina propria, immediately beneath and surrounding the crypts were counted. Three mice in each group were analyzed. H&E-stained intestinal sections were evaluated for tumor stage by a board-certified GI pathologist (Dr. SF Kuan).

Quantitative Reverse-transcription PCR analysis

Total RNA was extracted from the mucosal layer of the mouse intestine or HT-29 cells using the RNeasy Mini Kit (Qiagen). The DNase-treated RNA was reverse-transcribed using SuperScript III reverse transcriptase (Invitrogen). The PCR reactions were performed on the CFX Connect Real-Time PCR Detection System (Bio-Rad Laboratories) using SsoAdvanced Universal SYBR Green Supermix (Bio-Rad Laboratories). The PCR thermal cycle conditions were as follows: denature at 95 °C for 30 s and 40 cycles for 95 °C, 10 s; 60 °C, 30 s. The specificity of the PCR products was determined by the melting curve analysis. *β-actin* was selected as an internal reference gene. The sequences of PCR primers are shown in Supplementary Table 3.

Senescence-associated (SA) β-Galactosidase Staining

After the mice were euthanized, the cecum was immediately removed and rinsed with ice-cold PBS. The tissues were frozen in dry ice after the excess liquid was carefully removed using filter paper. Then the tissues were embedded in OCT compound and cut into 10-μm sections. The assays were performed using the Senescence β-Galactosidase Staining Kit (Cell Signaling Technology) according to the manufacturer's instructions. The sections were counterstained with hematoxylin before being dehydrated and coverslipped with mounting media.

MSI Analysis

The DNA was extracted from FFPE tissue sections using QIAamp DNA FFPE Tissue Kit (Qiagen). Cecal hyperplasia samples were from 6-week-old *FBC* mice. Cecal tumor samples were from 9-14.5-month-old *FBC* mice. Cecal tissue of 6-week-old *B* mice was used as control. According to a prior report [61], five microsatellite repeat markers, Bat24, Bat26, Bat30, Bat37 and Bat64, were used for MSI analysis. PCR amplification was carried out in a multiplex reaction using HSTaq polymerase (Takara Bio, Japan), with primer concentrations 0.5 μM. The thermal cycling conditions were as follows: initial denaturation at 95°C for 5 minutes; followed by 35 cycles of 95°C for 30 s, 60°C for 30 s, and 72°C for 30 s; then a final extension step at 68°C for 30 minutes. PCR fragments were analyzed by capillary electrophoresis, ABI3130XL (Life Technologies), and the GeneMapper ID3.2 program (Life Technologies). Tumor samples with greater or equal 40% MSI were classified as MSI-high (MSI-H), less than 40% as MSI-low (MSI-L), and samples without alterations were classified as MSS.

RNA-seq and data analysis

Total RNA was extracted from the cecal tissues of indicated mice using the RNeasy Mini Kit (Qiagen). After DNase I treatment and performing quality control (QC), 200 ng of high-quality total RNA was proceeded to library construction. Oligo(dT) magnetic beads were used to isolate mRNA. The mRNA was fragmented randomly by adding fragmentation buffer, then the cDNA was synthesized using mRNA template and random hexamers primer. Short fragments are purified

and resolved with EB buffer for end repair and single nucleotide A (adenine) addition. After that, the short fragments were connected to sequencing adapters. The double-stranded cDNA library was completed through size selection and PCR enrichment. Agilent 2100 Bioanaylzer and ABI StepOnePlus Real-Time PCR System were used in the quantification and qualification of the sample library. Finally, the qualified RNA-seq libraries were sequenced using Illumina NovaSeq6000 in CD Genomics (Shirley, NY) after pooling according to its effective concentration and expected data volume. The FastQC tool was used to perform basic statistics on the quality of the raw reads. Sequencing adapters and low-quality data were removed by Cutadapt (version 1.17). The alignment tool Salmon (version 0.13.1) was employed to quantify transcript expression based on mm10 reference genome. Output files from Salmon were imported into R (V.4.2.0) and analyzed by DESeq2 package (V1.36.0) to identify differentially expressed genes. All genes were ranked by log2(fold change) and used to check the gene set enrichment by using clusterProfiler[4] (V.4.4.1) in R. The following gene sets were used: MAPK signature [20]; intestinal Wnt signature [35]; cancer YAP/TAZ target gene signature [36]; intestinal differentiation signature [37]; intestinal stem cell signature [38]; the Hallmark Inflammatory Response gene set (Broad Institute) [34]; upregulated fetal spheroid markers [41]; upregulated and downregulated genes in human SSA/P [31] (only genes in human SSA/Ps with fold increase>2 or fold decrease<-2 with FDR<0.05 were used).

Whole exome sequencing

DNA was extracted from the cecal tumor of 12-month-old *FBC* mice using DNeasy Blood & Tissue Kits (Qiagen). Sequencing libraries were generated using Agilent SureSelect mouse All Exon Kit (Agilent Technologies) following the manufacturer's instructions and index codes were added to attribute sequences to each sample. DNA samples were sonicated using a hydrodynamic shearing system (Covaris) to generate 180-280bp fragments. The remaining DNA overhangs were converted into blunt ends by exonuclease/polymerase. After the adenylation of 3' ends, DNA fragments were ligated with adapter oligonucleotides. The fragments with adapters on both ends were selectively enriched using PCR. Then the library was hybridized in the liquid phase with biotin-labeled probes, followed by the capture of the exons using streptomycin-coated magnetic beads. Captured libraries were enriched by PCR to add index tags to prepare for hybridization. The resulting products were then purified using the AMPure XP System (Beckman Coulter) and quantified using the Agilent High Sensitivity DNA Assay on the Agilent Bioanalyzer 2100 System. The qualified libraries were sequenced using Illumina NovaSeq6000 in CD Genomics (Shirley, NY) after pooling according to its effective concentration and expected data volume. For the alignment step, BWA is utilized to perform reference genome alignment with the reads contained in paired FASTQ files. For the first post-alignment processing step, Picard tools are utilized to identify and mark duplicate reads from BAM file. The variant calling was performed by using GATK HaplotypeCaller.

Analysis of CRC patient data

TCGA RNA-seq data and mutation data of all cancer types were collected from Xena database (*https://xenabrowser.net/datapages/*), i.e., TCGA Pan-Cancer (PANCAN), which includes 376 CRC tumor samples and 51 matched normal samples. Expression data for *FAK* and mutation data for *BRAF* were extracted for analysis. The difference between the two groups was evaluated using the Student *t*-test (two-tailed, pairwise).

Author contributions

Conceptualization: CG, EC, JH

Investigation: CG, HG, SFK, CC, XL, JW, FE, JH

Visualization: CG, HG, CC, XL, JH

Funding acquisition: FE, JH

Supervision: EC, JH

Writing – original draft: CG, JH

Writing – review & editing: CG, RES, EC, JH

Data and materials availability

All data are available in the main text or supplementary materials.

References

1 Powell S. M., et al. (1992) **APC mutations occur early during colorectal tumorigenesis** *Nature* **359**:235–237 https://doi.org/10.1038/359235a0

2 Cancer Genome Atlas N. (2012) **Comprehensive molecular characterization of human colon and rectal cancer** *Nature* **487**:330–337 https://doi.org/10.1038/nature11252

3 Rad R., et al. (2013) **A genetic progression model of Braf(V600E)-induced intestinal tumorigenesis reveals targets for therapeutic intervention** *Cancer Cell* **24**:15–29 https://doi.org/10.1016/j.ccr.2013.05.014

4 Carragher L. A., et al. (2010) **V600EBraf induces gastrointestinal crypt senescence and promotes tumour progression through enhanced CpG methylation of p16INK4a** *EMBO Mol Med* **2**:458–471 https://doi.org/10.1002/emmm.201000099

5 Rustgi A. K. (2013) **BRAF: a driver of the serrated pathway in colon cancer** *Cancer Cell* **24**:1–2 https://doi.org/10.1016/j.ccr.2013.06.008

6 Lannagan T. R. M., et al. (2018) **Genetic editing of colonic organoids provides a molecularly distinct and orthotopic preclinical model of serrated carcinogenesis** *Gut* https://doi.org/10.1136/gutjnl-2017-315920

7 Davies H., et al. (2002) **Mutations of the BRAF gene in human cancer** *Nature* **417**:949–954 https://doi.org/10.1038/nature00766

8 Morin P. J., et al. (1997) **Activation of beta-catenin-Tcf signaling in colon cancer by mutations in beta-catenin or APC** *Science* **275**:1787–1790 https://doi.org/10.1126/science.275.5307.1787

9 Albuquerque C., et al. (2002) **The 'just-right' signaling model: APC somatic mutations are selected based on a specific level of activation of the beta-catenin signaling cascade** *Hum Mol Genet* **11**:1549–1560 https://doi.org/10.1093/hmg/11.13.1549

10 Leedham S. J., et al. (2013) **A basal gradient of Wnt and stem-cell number influences regional tumour distribution in human and mouse intestinal tracts** *Gut* **62**:83–93 https://doi.org/10.1136/gutjnl-2011-301601

11 Christie M., et al. (2013) **Different APC genotypes in proximal and distal sporadic colorectal cancers suggest distinct WNT/beta-catenin signalling thresholds for tumourigenesis** *Oncogene* **32**:4675–4682 https://doi.org/10.1038/onc.2012.486

12 Buchert M., et al. (2010) **Genetic dissection of differential signaling threshold requirements for the Wnt/beta-catenin pathway in vivo** *PLoS Genet* **6** https://doi.org/10.1371/journal.pgen.1000816

13 Wellbrock C., Karasarides M., Marais R. (2004) **The RAF proteins take centre stage** *Nat Rev Mol Cell Biol* **5**:875–885 https://doi.org/10.1038/nrm1498

14 Riemer P., et al. (2015) **Transgenic expression of oncogenic BRAF induces loss of stem cells in the mouse intestine, which is antagonized by beta-catenin activity** *Oncogene* **34**:3164–3175 https://doi.org/10.1038/onc.2014.247

15 Tong K., et al. (2017) **Degree of Tissue Differentiation Dictates Susceptibility to BRAF-Driven Colorectal Cancer** *Cell Rep* **21**:3833–3845 https://doi.org/10.1016/j.celrep.2017.11.104

16 Brandt R., et al. (2019) **Cell type-dependent differential activation of ERK by oncogenic KRAS in colon cancer and intestinal epithelium** *Nat Commun* **10** https://doi.org/10.1038/s41467-019-10954-y

17 Zebisch A., Troppmair J. (2006) **Back to the roots: the remarkable RAF oncogene story** *Cell Mol Life Sci* **63**:1314–1330 https://doi.org/10.1007/s00018-006-6005-y

18 Rajagopalan H., et al. (2002) **Tumorigenesis: RAF/RAS oncogenes and mismatch-repair status** *Nature* **418** https://doi.org/10.1038/418934a

19 Lake D., Correa S. A., Muller J. (2016) **Negative feedback regulation of the ERK1/2 MAPK pathway** *Cell Mol Life Sci* **73**:4397–4413 https://doi.org/10.1007/s00018-016-2297-8

20 Pratilas C. A., et al. (2009) **(V600E)BRAF is associated with disabled feedback inhibition of RAF-MEK signaling and elevated transcriptional output of the pathway** *Proc Natl Acad Sci U S A* **106**:4519–4524 https://doi.org/10.1073/pnas.0900780106

21 Yao Z., et al. (2015) **BRAF Mutants Evade ERK-Dependent Feedback by Different Mechanisms that Determine Their Sensitivity to Pharmacologic Inhibition** *Cancer Cell* **28**:370–383 https://doi.org/10.1016/j.ccell.2015.08.001

22 Corcoran R. B., et al. (2012) **EGFR-mediated re-activation of MAPK signaling contributes to insensitivity of BRAF mutant colorectal cancers to RAF inhibition with vemurafenib** *Cancer Discov* **2**:227–235 https://doi.org/10.1158/2159-8290.CD-11-0341

23 Prahallad A., et al. (2012) **Unresponsiveness of colon cancer to BRAF(V600E) inhibition through feedback activation of EGFR** *Nature* **483**:100–103 https://doi.org/10.1038/nature10868

24 Sulzmaier F. J., Jean C., Schlaepfer D. D. (2014) **FAK in cancer: mechanistic findings and clinical applications** *Nat Rev Cancer* **14**:598–610 https://doi.org/10.1038/nrc3792

25 Pylayeva Y., et al. (2009) **Ras- and PI3K-dependent breast tumorigenesis in mice and humans requires focal adhesion kinase signaling** *The Journal of clinical investigation* **119**:252–266 https://doi.org/10.1172/JCI37160

26 Luo M., et al. (2009) **Mammary epithelial-specific ablation of the focal adhesion kinase suppresses mammary tumorigenesis by affecting mammary cancer stem/progenitor cells** *Cancer research* **69**:466–474 https://doi.org/10.1158/0008-5472.CAN-08-3078

27 Ashton G. H., et al. (2010) **Focal adhesion kinase is required for intestinal regeneration and tumorigenesis downstream of Wnt/c-Myc signaling** *Dev Cell* **19**:259–269 https://doi.org/10.1016/j.devcel.2010.07.015

28 McLean G. W., et al. (2004) **Specific deletion of focal adhesion kinase suppresses tumor formation and blocks malignant progression** *Genes & development* **18**:2998–3003 https://doi.org/10.1101/gad.316304

29 Shang N., et al. (2014) **FAK is required for c-Met/beta-catenin-driven hepatocarcinogenesis** *Hepatology* https://doi.org/10.1002/hep.27402

30 Clarke C. N., Kopetz E. S. (2015) **BRAF mutant colorectal cancer as a distinct subset of colorectal cancer: clinical characteristics, clinical behavior, and response to targeted therapies** *J Gastrointest Oncol* **6**:660–667 https://doi.org/10.3978/j.issn.2078-6891.2015.077

31 Kanth P., et al. (2016) **Gene Signature in Sessile Serrated Polyps Identifies Colon Cancer Subtype** *Cancer Prev Res (Phila)* **9**:456–465 https://doi.org/10.1158/1940-6207.CAPR-15-0363

32 Tong K., et al. (2021) **SMAD4 is critical in suppression of BRAF-V600E serrated tumorigenesis** *Oncogene* **40**:6034–6048 https://doi.org/10.1038/s41388-021-01997-x

33 Leach J. D. G., et al. (2021) **Oncogenic BRAF, unrestrained by TGFbeta-receptor signalling, drives right-sided colonic tumorigenesis** *Nat Commun* **12** https://doi.org/10.1038/s41467-021-23717-5

34 Liberzon A., et al. (2015) **The Molecular Signatures Database (MSigDB) hallmark gene set collection** *Cell Syst* **1**:417–425 https://doi.org/10.1016/j.cels.2015.12.004

35 Van der Flier L. G., et al. (2007) **The Intestinal Wnt/TCF Signature** *Gastroenterology* **132**:628–632 https://doi.org/10.1053/j.gastro.2006.08.039

36 Wang Y., et al. (2018) **Comprehensive Molecular Characterization of the Hippo Signaling Pathway in Cancer** *Cell Rep* **25**:1304–1317 https://doi.org/10.1016/j.celrep.2018.10.001

37 Chong J. L., et al. (2009) **E2f1-3 switch from activators in progenitor cells to repressors in differentiating cells** *Nature* **462**:930–934 https://doi.org/10.1038/nature08677

38 Munoz J., et al. (2012) **The Lgr5 intestinal stem cell signature: robust expression of proposed quiescent '+4' cell markers** *EMBO J* **31**:3079–3091 https://doi.org/10.1038/emboj.2012.166

39 Glinka A., et al. (2011) **LGR4 and LGR5 are R-spondin receptors mediating Wnt/beta-catenin and Wnt/PCP signalling** *EMBO Rep* **12**:1055–1061 https://doi.org/10.1038/embor.2011.175

40 de Lau W., et al. (2011) **Lgr5 homologues associate with Wnt receptors and mediate R-spondin signalling** *Nature* **476**:293–297 https://doi.org/10.1038/nature10337

41 Mustata R. C., et al. (2013) **Identification of Lgr5-independent spheroid-generating progenitors of the mouse fetal intestinal epithelium** *Cell Rep* **5**:421–432 https://doi.org/10.1016/j.celrep.2013.09.005

42 Kabiri Z., et al. (2018) **Wnt signaling suppresses MAPK-driven proliferation of intestinal stem cells** *J Clin Invest* **128**:3806–3812 https://doi.org/10.1172/JCI99325

43 Sieg D. J., et al. (2000) **FAK integrates growth-factor and integrin signals to promote cell migration** *Nat Cell Biol* **2**:249–256 https://doi.org/10.1038/35010517

44 Mancini A., et al. (2020) **LGR4 deficiency results in delayed puberty through impaired Wnt/beta-catenin signaling** *JCI Insight* **5** https://doi.org/10.1172/jci.insight.133434

45 Bennecke M., et al. (2010) **Ink4a/Arf and oncogene-induced senescence prevent tumor progression during alternative colorectal tumorigenesis** *Cancer Cell* **18**:135–146 https://doi.org/10.1016/j.ccr.2010.06.013

46 Amodio V., et al. (2020) **EGFR Blockade Reverts Resistance to KRAS(G12C) Inhibition in Colorectal Cancer** *Cancer Discov* **10**:1129–1139 https://doi.org/10.1158/2159-8290.CD-20-0187

47 Yaeger R., Corcoran R. B. (2019) **Targeting Alterations in the RAF-MEK Pathway** *Cancer Discov* **9**:329–341 https://doi.org/10.1158/2159-8290.CD-18-1321

48 Wan P. T., et al. (2004) **Mechanism of activation of the RAF-ERK signaling pathway by oncogenic mutations of B-RAF** *Cell* **116**:855–867 https://doi.org/10.1016/s0092-8674(04)00215-6

49 Michaloglou C., et al. (2005) **BRAFE600-associated senescence-like cell cycle arrest of human naevi** *Nature* **436**:720–724 https://doi.org/10.1038/nature03890

50 Dankort D., et al. (2007) **A new mouse model to explore the initiation, progression, and therapy of BRAFV600E-induced lung tumors** *Genes Dev* **21**:379–384 https://doi.org/10.1101/gad.1516407

51 Sarkisian C. J., et al. (2007) **Dose-dependent oncogene-induced senescence in vivo and its evasion during mammary tumorigenesis** *Nat Cell Biol* **9**:493–505 https://doi.org/10.1038/ncb1567

52 Murphy D. J., et al. (2008) **Distinct thresholds govern Myc's biological output in vivo** *Cancer Cell* **14**:447–457 https://doi.org/10.1016/j.ccr.2008.10.018

53 Land H., Parada L. F., Weinberg R. A. (1983) **Tumorigenic conversion of primary embryo fibroblasts requires at least two cooperating oncogenes** *Nature* **304**:596–602 https://doi.org/10.1038/304596a0

54 Viros A., et al. (2014) **Ultraviolet radiation accelerates BRAF-driven melanomagenesis by targeting TP53** *Nature* **511**:478–482 https://doi.org/10.1038/nature13298

55 Kidger A. M., et al. (2017) **Dual-specificity phosphatase 5 controls the localized inhibition, propagation, and transforming potential of ERK signaling** *Proc Natl Acad Sci U S A* **114**:E317–E326 https://doi.org/10.1073/pnas.1614684114

56 Unni A. M., et al. (2018) **Hyperactivation of ERK by multiple mechanisms is toxic to RTK-RAS mutation-driven lung adenocarcinoma cells** *Elife* **7** https://doi.org/10.7554/eLife.33718

57 Bollag G., et al. (2010) **Clinical efficacy of a RAF inhibitor needs broad target blockade in BRAF-mutant melanoma** *Nature* **467**:596–599

58 Kopetz S., et al. (2019) **Encorafenib, Binimetinib, and Cetuximab in BRAF V600E-Mutated Colorectal Cancer** *N Engl J Med* **381**:1632–1643 https://doi.org/10.1056/NEJMoa1908075

59 Batlle E., Clevers H. (2017) **Cancer stem cells revisited** *Nat Med* **23**:1124–1134 https://doi.org/10.1038/nm.4409

60 Sugimoto S., Sato T. (2017) **Establishment of 3D Intestinal Organoid Cultures from Intestinal Stem Cells** *Methods Mol Biol* **1612**:97–105 https://doi.org/10.1007/978-1-4939-7021-6_7

61 Nakanishi Y., et al. (2018) **Simultaneous Loss of Both Atypical Protein Kinase C Genes in the Intestinal Epithelium Drives Serrated Intestinal Cancer by Impairing Immunosurveillance** *Immunity* **49**:1132–1147 https://doi.org/10.1016/j.immuni.2018.09.013

Article and author information

Chenxi Gao
Division of Gastroenterology, Hepatology and Nutrition, Department of Medicine, University of Pittsburgh School of Medicine, Pittsburgh, PA 15213

Huaibin Ge
UPMC Hillman Cancer Center, Division of Hematology and Oncology, Department of Medicine, University of Pittsburgh, Pittsburgh, PA, 15213, USA

Shih-Fan Kuan
Department of Pathology, University of Pittsburgh School of Medicine, Pittsburgh, PA 15213

Chunhui Cai
Department of Biomedical Informatics, University of Pittsburgh, Pittsburgh, PA 15206

Xinghua Lu
Department of Biomedical Informatics, University of Pittsburgh, Pittsburgh, PA 15206
ORCID iD: 0000-0002-8599-2269

Farzad Esni
Department of Surgery, University of Pittsburgh School of Medicine, Pittsburgh, PA 15213
ORCID iD: 0000-0002-0342-6862

Robert E. Schoen
Division of Gastroenterology, Hepatology and Nutrition, Department of Medicine, University of Pittsburgh School of Medicine, Pittsburgh, PA 15213
ORCID iD: 0000-0001-7153-2766

Jing H. Wang
UPMC Hillman Cancer Center, Division of Hematology and Oncology, Department of Medicine, University of Pittsburgh, Pittsburgh, PA, 15213, USA
ORCID iD: 0000-0003-4343-2527

Edward Chu
UPMC Hillman Cancer Center, Division of Hematology and Oncology, Department of Medicine, University of Pittsburgh, Pittsburgh, PA, 15213, USA, Current address: Albert Einstein Cancer Center, Albert Einstein College of Medicine, Bronx, NY 10461

Jing Hu
Division of Gastroenterology, Hepatology and Nutrition, Department of Medicine, University of Pittsburgh School of Medicine, Pittsburgh, PA 15213
For correspondence: huj3@upmc.edu

Copyright

© 2024, Gao et al.

This article is distributed under the terms of the Creative Commons Attribution License, which permits unrestricted use and redistribution provided that the original author and source are credited.

Editors

Reviewing Editor
Patrick Hu
Vanderbilt University Medical Center, Nashville, United States of America

Senior Editor
Richard White
Ludwig Institute for Cancer Research, University of Oxford, Oxford, United Kingdom

Reviewer #1 (Public Review):

Summary:

The authors provide solid evidence with a mouse model as well as supporting in vitro and analysis of clinical samples that loss of Fak increases the development of BRAF V600E-induced dysplastic lesions and carcinomas in the cecum via downregulation of Egfr-mediated Erk phosphorylation. This fine-tuning of Erk phosphorylation increases the expression of Lrg4 mRNA expression and promotes Lrg4 stability through downregulation of the E3 ubiquitin ligase Nedd4. The high Lrg4 expression correlates with an increased intestinal stem cell transcriptional signature that the authors suggest drives higher rates of transformation. This provides important insight that factors such as FAK may be able to modulate MAPK-driven tumorigenesis in specific circumstances. The data presented here are largely specific to the cecum. While these specific findings may ultimately have practical implications for human CRC outside the cecum and even therapeutic implications, these remain unexplored and will be a point for future investigations.

Strengths:

The authors use a mouse model (intestinal specific BRAF V600E +/- Fak knockout) as well as supporting in vitro analyses and clinical sample characterization to support their model. For both in vitro and in vivo studies, the authors use a combination of genetic and pharmacologic (including EGFR, FAK, and MEK inhibitors) tools to modulate the MAPK pathway. They also use a combination of transcriptional (RNA-Seq) and protein (IHC and Western blotting) readouts to support their proposed model. Importantly, they use a distinct mouse model (mutant Kras) to demonstrate their findings with Fak loss are specific to instances where EGFR can modulate ERK activation, providing strong evidence for their model. Finally, they also correlate their findings in the murine model with patient samples and with trends in the TCGA database. Collectively, these create a solid and convincing basis for their proposed model.

Weaknesses:

(1) The murine data is largely confined to the cecum. While the analysis of the cecum is appropriate based on the cecum specificity of their phenotype, they often use these findings to make broader generalizations about the nature of tumorigenesis in the intestinal epithelia and in CRC more generally. In my opinion, there was insufficient evidence presented supporting the extension of the proposed model beyond the cecum. While this is a weakness,

it could be part of a growing effort to characterize left and right-sided malignancies as related but separate disease processes.

(2) The authors generally do a good job of focusing their analysis on the cecum and supporting their model. For example, Figure 5A examines different colon compartments, including the cecum. However, the authors fail to demonstrate that Fak loss only promotes Lrg4 upregulation in the cecum, where they observe an increase in BRAF V600E dysplasia and carcinoma. This is again seen in Figure 6A, where they only characterize Nedd4 expression in the cecum and not other compartments of the colon.

(3) The authors evaluate a broad range of tissues, including normal colonic mucosa, polyps, pre-cancerous dysplastic lesions, adenocarcinomas, and adenocarcinoma cell lines. While this breadth is a strength of the paper, the authors, at times, equate experimental observations in each of these conditions, despite the difference in the biology of these tissues/cells. For example, in their mouse model, they equate the development of dysplastic lesions and carcinoma lesions. This makes it difficult to accurately interpret their data and conclusions.

(4) In Figure 5i, this experiment was only completed in one cell line (HT29), despite the conclusion that Lrg4 expression is increased by decreased ERK phosphorylation due to protein stabilization. HT29 cells are a transformed human CRC cell line, quite different than a pre-malignant cecum intestinal epithelial cell. While convincing, the authors could have performed this key experiment in non-transformed murine cecal organoids (as they did for other experiments in Figure 5E), which would better recapitulate the mouse and pre-malignant setting to explain their mouse phenotype.

(5) While a large portion of the discussion focusses on the therapeutic implications of these findings, the authors only really investigate tumorigenesis. They likely have additional investigations planned for future manuscripts.

https://doi.org/10.7554/eLife.94605.1.sa2

Reviewer #2 (Public Review):

Summary:

The manuscript by Gao et al. described a study identifying the role of FAK in fine-tuning the activation levels of ERK signaling in BRAF-V600E-driven colorectal cancer. The authors generated new mouse models combining Vill-Cre mediated BRAF-V600E expression with FAK deletion. Analyses of intestinal tumor phenotypes revealed that FAK-loss promotes BRAF-V600E-induced tumor formation, specifically in the cecum. Interestingly, these tumors closely resemble human sessile serrated adenoma/polyps. Using bioinformatics analysis, the authors found that FAK deletion upregulates the intestinal stem cell and fetal-type transcriptomic signatures compared to mice expressing BRAF-V600E alone. In addition, FAK-loss decreases the phosphorylation of ERK whereas it increases the expression of Lgr4 at both mRNA and protein levels. To mechanistically connect FAK-mediated downregulation of ERK and upregulation of Lgr4 in the context of BRAF-V600E mutation, results from biochemical experiments showed that MEK inhibitor treatment decreases the expression of NEDD4, a previously identified ubiquitin E3 ligase of Lgr4, which coincides with increased Lgr4 protein expression both in cells and in vivo. Moreover, the FAK-dependent modulation of ERK signaling is specific to BRAF-V600E-driven tumorigenesis only as knockout of FAK has no effect in Vill-Cre/KRAS-G12D mice. Collectively, the authors proposed a "just right" model in that a tunable FAK expression controls the optimal level of ERK pathway output needed for BRAF-V600E-induced cecal tumor formation.

Strengths:

This study provides new insights into the mechanisms underlying the serrated pathway-driven tumorigenesis in colorectal cancer. The newly established mouse model with compound mutations of BRAF and FAK offers a useful resource for future studies of the serrated pathway. The conclusions of this paper are mostly supported by data.

Weaknesses:

However, some aspects of the paper can be strengthened with additional mechanistically focused experiments.

(1) Some of the conclusions of the paper mainly rely on bioinformatic analyses of RNA-seq data. For example, it has been noted in several places in the paper that the knockout of FAK in Vill-Cre/BRAF-V600E mice does not affect the transcriptional outcome downstream of ERK while ERK phosphorylation levels are decreased. This statement is based on the lack of significant difference in the MAPK signature according to GSEA. However, whereas a significant enrichment of certain pathways can be used as support evidence, the lack of enrichment does not necessarily indicate those pathways are not involved. Other experiments are needed to examine the expression of ERK target genes to confirm. Similarly, the upregulation of fetal stem cell signature in FAK knockout mice needs to be verified using other methods besides GSEA.

(2) According to Figure 5i, the half-life of Lgr4 is around 48 hours in HT29 cells. However, it has been reported by at least two other publications cited in this paper (Ref. 44 and 45) that the half-life of Lgr4 is much shorter. This discrepancy is not explained.

(3) The effect of decreased ERK signaling on NEDD4 expression has only been briefly explored in Figure 6. The mechanisms by which FAK-loss and/or inhibition of MEK/ERK activity regulate NEDD4 expression are currently unclear. Moreover, the levels of NEDD4 expression are only analyzed in one mouse per group in Figure 6a. Quantitative analysis of NEDD4 as well as Lgr4 expression in additional numbers of mice will provide more solid support for the inverse correlation between NEDD4 and Lgr4 proteins. Since MEK inhibitor treatment also increases Lgr4 mRNA expression as shown in Figure 5f-g, the relative contribution of this altered mRNA expression vs. NEDD4L-mediated ubiquitination has not been investigated.

(4) It is an interesting finding that knockout FAK has no effect on KRAS-G12D-driven hyperplasia as shown in Figure 7. However, additional studies are needed to further explore the potential mechanisms by which FAK-loss specifically decreases EGFR/ERK signaling in the context of BRAF-V600E mutation.

https://doi.org/10.7554/eLife.94605.1.sa1

Reviewer #3 (Public Review):

Summary:

Right-sided colorectal Cancer (CRC) is very different from left-sided CRC. Therefore it is important to model this cancer in mice and find new molecular targets. A broad set of data exists on FAK (Focal Adhesion Kinase) being important in colorectal cancer. However, this has focussed on APC mutant CRC which tends to be left-sided. BRAF mutation is common in right-sided CRC (and is rarely mutated with APC). Therefore the authors have tested whether FAK is important in this context. The authors show that FAK deletion surprisingly accelerates BRAF mutant CRC. Tumours arise in the proximal colon (which recapitulates BRAF mutant right-

sided CRC). There are low for Lgr5 and high for foetal programmes. Mechanistically they suggest a pathway from FAK to NEDD4 to Lgr4 may underpin this phenotype.

Strengths:

Strong genetic data from FAK revealed that there is an acceleration of tumourigenesis and mice now develop proximal colon tumours and can be viewed as a good model of right-sided CRC.
The expression data between humans and mice is strong.

Weaknesses:

The functional mechanism of how FAK loss promotes tumourigenesis is still quite correlative. An alternative hypothesis is that it drives inflammation in the proximal colon that drives tumourigenesis.

We still did not know the functional role for LGR4 (loss leads to a loss of paneth cells in homeostasis) so I'm not sure you can hypothesise a stem cell role.

https://doi.org/10.7554/eLife.94605.1.sa0